ORIGINAL RESEARCH

Optimized hybrid YOLOu-Quasi-ProtoPNet for insulators classification

Stefano Frizzo Stefenon[1,2] 🔵 | Gurmail Singh[3] | Bruno José Souza[4] |
Roberto Zanetti Freire[5] | Kin-Choong Yow[6]

[1]Digital Industry Center, Fondazione Bruno Kessler, Trento, Italy

[2]Department of Mathematics, Computer Science and Physics, University of Udine, Udine, Italy

[3]Department of Computer Sciences, University of Wisconsin-Madison, Madison, Wisconsin, USA

[4]Industrial and Systems Engineering Graduate Program (PPGEPS), Pontifical Catholic University of Parana (PUCPR), Curitiba, Brazil

[5]Universidade Tecnológica Federal do Paraná (UTFPR), Curitiba, Brazil

[6]Faculty of Engineering and Applied Science, University of Regina, Regina, Saskatchewan, Canada

Correspondence

Stefano Frizzo Stefenon, Digital Industry Center, Fondazione Bruno Kessler, Via Sommarive 18, Trento, TN 38123, Italy.
Email: sfrizzostefenon@fbk.eu

Abstract

To ensure the electrical power supply, inspections are frequently performed in the power grid. Nowadays, several inspections are conducted considering the use of aerial images since the grids might be in places that are difficult to access. The classification of the insulators' conditions recorded in inspections through computer vision is challenging, as object identification methods can have low performance because they are typically pre-trained for a generalized task. Here, a hybrid method called YOLOu-Quasi-ProtoPNet is proposed for the detection and classification of failed insulators. This model is trained from scratch, using a personalized ultra-large version of YOLOv5 for insulator detection and the optimized Quasi-ProtoPNet model for classification. For the optimization of the Quasi-ProtoPNet structure, the backbones VGG-16, VGG-19, ResNet-34, ResNet-152, DenseNet-121, and DenseNet-161 are evaluated. The F1-score of 0.95165 was achieved using the proposed approach (based on DenseNet-161) which outperforms models of the same class such as the Semi-ProtoPNet, Ps-ProtoPNet, Gen-ProtoPNet, NP-ProtoPNet, and the standard ProtoPNet for the classification task.

1 | INTRODUCTION

Insulators in the transmission lines are components responsible for supporting the electrical power grid and isolating the electrical potential [1]. When there is an accumulation of contamination on the surface of these components, electrical discharges may occur [2–4]. Contamination is difficult to measure because its presence does not represent an imminent failure, besides the rain can help clean the insulators [5]. Over time the contamination becomes encrusted and strongly attached to the surface of insulators, causing these components to lose their insulating properties [6]. Apart from contamina-

tion, insulators are vulnerable to vandalism and other issues because they are mostly installed outdoors [7–9].

When insulators lose their insulating properties intermittent discharges can happen, affecting power quality [10]. With increasing partial discharges and leakage current [11], the condition can worsen until disruptive discharges occur, resulting in the shutdown of the power grid [12]. In many cases after a shutdown, the system is re-established and the fault does not have the same features (distribution of the contamination over the insulation surface), which makes it difficult to locate. The electrical outage represents a serious problem for the reliability of the electricity supply [13], reducing the power quality indices

that are used to measure whether the electric utility is adequately serving consumers [14].

To mitigate electrical system shutdowns, inspections are carried out by specialized teams to identify signs of adverse conditions [15]. Power system examinations can be performed using specific equipment or visual inspections [16]. The equipment that is generally used in inspections are acoustic detectors [17], ultraviolet sensors [18], infrared cameras [19], and others [20]. One of the disadvantages of using this specific type of equipment is that the operator needs to be specialized in its operation having the ability to interpret a possible indication of a failure, which is difficult due to the need for multitasking operators [21].

Among the image processing techniques for classification, convolutional neural networks (CNNs) have been widely used for pattern recognition [22], highlighting specific applications for electrical power system fault identification [23]. There are several variations of these models and their applications are promising for the identification of adverse conditions in the power grid. Currently available, there is the prototypical part network (ProtoPNet), which as a major advantage has interpretability in some cases, beyond improving the classification can assist in the interpretation of the result. Based on this characteristic, the ProtoPNet is promising to solve the problem of classification presented here.

Generally, CNNs have difficulties identifying small objects, you only look once (YOLO) stands out to solve this task [24], having a better performance than sliding windows methods based on standard CNNs [25]. Considering that the YOLO model has a high capacity to detect objects and the ProtoPNet approach has a higher classification capacity, here, we propose the hybrid optimized YOLOu-Quasi-ProtoPNet that combines the best advantages of each class of these models. The contributions of this paper are:

- The first contribution is the object detection performance improvement of the YOLOv5 model proposing a personalized ultra-large version (YOLOv5u), which has proven superior to the variations of the standard YOLOv5 models (YOLOv5n, YOLOv5s, YOLOv5m, YOLOv5l, and YOLOv5x).
- The second contribution is related to the use of a hybrid approach, which uses the best capabilities of the YOLOv5u for object detection and a Quasi-ProtoPNet model for classification. Considering the evaluation of VGG-16, VGG-19, ResNet-34, ResNet-152, DenseNet-121, and DenseNet-161 as backbone.
- The third advantage of the proposed model is its explainability. The explainability helps the users to understand why the model performs the classification, helping the maintenance teams work on the need. The Quasi-ProtoPNet uses prototypes of large spatial dimensions that help the model classify images based on objects rather than the backgrounds of the objects in the images.

The rest of this paper is organized as follows: In Section 2 related works regarding insulator fault detection using

computer vision are presented. Section 3 presents the proposed YOLOu-Quasi-ProtoPNet model. In Section 4 the structure optimization of the model and fine-tuning are presented and discussed. In Section 5 the final considerations are presented and further works are suggested.

2 | RELATED WORKS

The evaluation of transmission power system insulators through inspections is important to keep the power grid in good working condition [26]. Several authors have been researching state-of-the-art models to improve network inspections [27–29]. Although network monitoring is efficient using specific equipment, in some situations it is unfeasible to take measurements in hard-to-access places, which can be solved by visual inspections [30]. The use of computer vision becomes a promising alternative to obtain a model that is effective in identifying adventitious conditions in the electrical power grid [31].

Besides porcelain insulators, glass insulators, and polymeric insulators can be found in electrical power transmission lines. Glass insulators have similar characteristics to porcelain insulators, considering that these materials have a high fusion temperature, which results in greater robustness to electric discharges [32], and therefore, they are the most common in electrical networks that are in operation for a long time (over 30 years). Polymeric insulators have been recently used because they are lighter, making them easier to install and perform maintenance [33]. The model proposed here could be applied to other types of profiles and materials, beyond those evaluated in this work, being necessary to train the model with the insulators in question.

According to Salem et al. [34], the insulator profile has an influence on its performance. They have evaluated insulators coated with room-temperature vulcanizing considering the influence of humidity on flashover based on the evaluation of different profiles. Salem et al. [35], using finite element methods (FEM), presented interesting results regarding the difference of profiles using glass insulators. They have highlighted that the issue depends on the location and dimension of the pollution region. FEMs have been applied to evaluate the design of power system components by simulating dynamic variations and optimizing the component's structure [36], making it promising for the definition of the insulator design [37, 38] and its ability to support stress [39].

Due to the popularization of unmanned aerial vehicles (UAVs), it is becoming increasingly common to use these types of aircraft to perform image-based monitoring of the power grid [40]. The main advantage of this approach is that UAVs can perform grid inspection in hard-to-reach places. Field teams that travel along the branch line taking photographs have a hard time doing this work when there is a large variation in relief, making the inspection unfeasible in some situations. For this reason, the use of UAVs is a promising alternative for power system inspection [41].

According to Foudeh et al. [42], one of the major difficulties in performing inspections in electrical power systems is

the lack of adaptability to adverse conditions, thus the use of UAVs has received much attention for overhead electric power lines patrol process. Due to the aging of composite insulators, the phenomenon of micro-cracks occurs, which can be identified with UAVs through image analysis. Jin et al. [43] show that through image pre-processing techniques it is possible to extract the texture of micro-cracks and identify them easily.

Another strategy that can be applied to improve the classification of adherent conditions in insulators is image pre-processing. In many situations, filters can be used to take the focus of the analysis of the background of the image and concentrate the evaluation on the fault locations. Edge detection techniques such as Sobel and Canny edge detection can be used to highlight the presence of faults, thus improving classification without representing a significant computational effort increase [44].

The fusion convolutional network (FCN) is an outstanding model for real-time monitoring of the power grid via UAVs. The FCN model proposed by Mussina et al. [45] consists of a CNN combined with a binary classifier multilayer neural network. By using the FCN model for a multi-modal information fusion system, the image classification output of the CNN can be combined with the leakage current values, thus obtaining a model with high classification capability. Among the CNNs, models based on VGG-16 [46], ResNet-101 [47], and AlexNet [48] have been used for this task.

The models that have stood out for object detection are the YOLOs because their architecture is based on a single shot and generally has better performance results than other models for the same application [49]. With this advantage, this model proves to be promising for the task being presented here. However, since the YOLO models are based on a standard backbone classifier that in versions YOLOv3 and YOLOv4 are based on Darknet53, it may have low classification performance when few images are used for training. To improve this problem, a hybrid method that uses another classifier may be an alternative to improve the fault identification capability of this class of models.

For image classification tasks, often the reasoning can be based on prototypical aspects of a class. Evidence of this difference aids the final decision [50]. The ProtoPNet dissects the image by finding prototypical parts and combines evidence from the prototypes to make a classification. Based on this advantage, the combination of the YOLO model for object detection with a model based on ProtoPNet becomes a promising proposal for the challenge presented here, and this model will be presented in more detail in the next section.

3 | YOLOu-QUASI-ProtoPNet

Considering the high performance of the YOLOv5 for object detection and the high classification capability of the Quasi-ProtoPNet model, here a hybrid model called YOLOu-Quasi-ProtoPNet is proposed. The structure of the proposed model is presented in Figure 1, which is divided into steps from A to F and is explained in detail in this section.

To improve the proposed method, an optimization of the network structure is performed by changing its classifier, in which VGG-16, VGG-19, ResNet-34, ResNet-152, DenseNet-121, and DenseNet-161 are evaluated. In Figure 1a, the images of the dataset are loaded, and the detection of insulators is performed using YOLOv5, wherein the structure size variations are evaluated (YOLOv5n, YOLOv5s, YOLOv5m, YOLOv5l, YOLOv5x, and YOLOv5u).

3.1 | You only look once

YOLO is a CNN that splits images into grids, having each grid cell detect objects within itself [51]. This approach is a single-shot algorithm, which means that it only requires processing the image once to detect and classify the object under consideration. Recently the YOLO has shown satisfactory results, and the framework has been improved several times since its initial release [52].

The input images are divided into an $S \times S$ grid, where each square of the grid (i) predicts the target bounding box, which corresponds to its degree of confidentiality. Therefore, the confidence of the classes (cl) of objects (obj), is given by:

$$pr(cl_i|obj) \cdot pr(obj) \cdot IoU_{pred}^{truth} = pr(cl_i) \cdot IoU_{pred}^{truth}. \quad (1)$$

After splitting the image into grids a class probability mean average precision (mAP) is created to identify the target objects and bounding boxes to determine if the desired objects are located in this confidence region. The YOLOv5 backbone has its structure (presented in Figure 1b), different from previous versions of the model which use the Darknet-53, this makes this version more effective and flexible to be modified according to the needs of the project.

The YOLOv5 framework has features that makes it promising for fault classification in insulators. The YOLOv5 applies Mosaic to improve the detection performance of small objects, which is a difficulty when inspections of insulators are carried out, considering that the failure may be small in relation to the insulator chain.

Using Mosaic, an increase in the data amount is introduced into the network training process, which consequently allows the increase of the batch size, causing each iteration to have more data. This feature might be an advantage in terms of having additional information to the model, however, it results in an increase in the need for data processing power. Since the training is performed offline, the higher computation effort in network training does not represent a disadvantage. The application of Mosaic reduces the size of the target and therefore increases the detection efficiency of smaller objects, which is a requirement to obtain applicable results [53].

YOLOv5 employs the Focus, BottleneckCSP, SPP, and path aggregation network (PANet) techniques to improve object
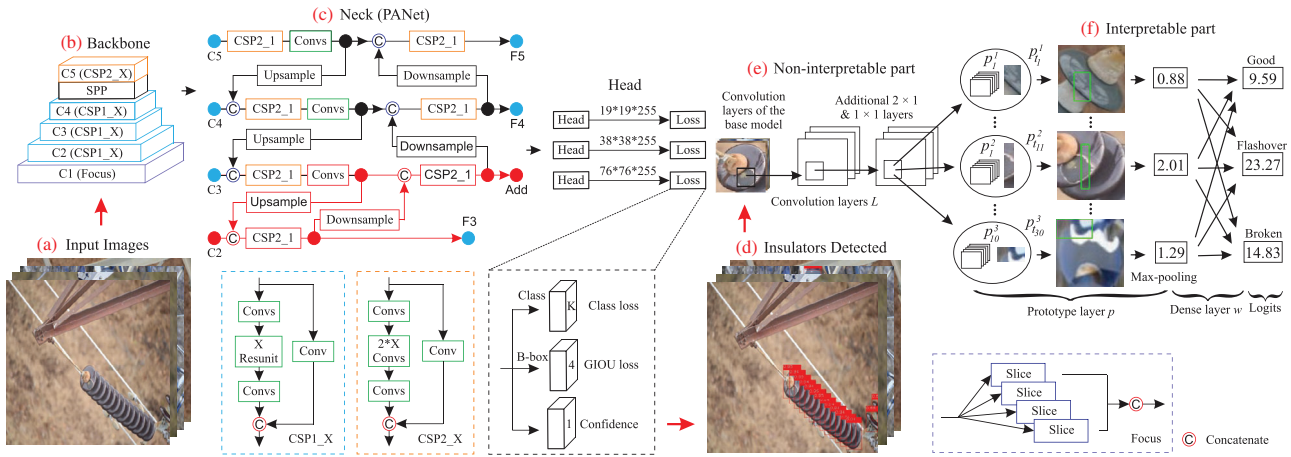
FIGURE 1 Structure of the proposed YOLOu-Quasi-ProtoPNet.

detection. Focus is applied to improve the receptive field, BottleneckCSP extracts the information from features, and SPP separates the features that are relevant to improve the nonlinear representation of the network. PANet combines the high and low-level features to enhance the accuracy detection, PANet improvement is highlighted in red in Figure 1c.

For better accuracy, it is common to scale a baseline detector using a bigger backbone network. The EfficientDet method [54], applied in YOLOv5, uses a bi-directional weighted feature pyramid network (BiFPN) for multiscale feature fusion and a composite scaling strategy that uniformly scales the resolution of the network, hence it jointly scales all dimensions of the backbone. The multiple depth is responsible for the depth of the model, meaning that it ends up adding more layers to the net, whereas the multiple width adds more filters to the layers, thus it adds more channels to the outputs of the layers. The *depth_width* parameters are responsible for defining the size of the network and creating the variations of the YOLOv5 models, these parameters will be evaluated here for proposing a custom model.

The proposed personalized ultra-large version of YOLOv5, named YOLOv5u emerged from the consideration that larger models have better mAP results in preliminary experiments presented by Ultralytics.[1] A progression in classification capability is observed when increasing network size, for this reason, a model larger than YOLOv5x seems promising, with YOLOv5x having the best results compared to other models with fewer parameters such as YOLOv5n, YOLOv5s, YOLOv5m, and YOLOv5l. The results of these models are based on a pretrained dataset using the common objects in context (COCO) [55]. Here, all these models were trained from scratch to have a fair comparison.

The disadvantage of using an ultra-large model is that it requires more powerful hardware, and has higher FLOPs, an approach that results in higher computational effort and more time needed for training. However, this is not a problem here,

since the training is performed offline, and the model has high speed in the testing phase. To create the YOLOv5u, the size of the net was changed and evaluated based on the variation of depth and width multiple, which is the variation performed in other YOLOv5 versions. The cross-entropy loss function is defined to calculate the score loss in object detection [56]. YOLOv5u creates a bounding box of the detected insulator (Figure 1d) that is validated by its confidence, and the crop-outs from it are made, these are the outputs of the YOLOv5u. After object detection, the outputs are classified by the Quasi-ProtoPNet model. For CNN models, a batch size multiple of 8 was used. The batch sizes were dependent on the base model, the heavier the base model the smaller the batch size. VGG-16, VGG-19, ResNet-34: batch size = 48, DenseNet-121: batch size = 32, DenseNet-161: batch size = 24, ResNet-152: batch size = 16.

3.2 | Quasi-ProtoPNet

Quasi-ProtoPNet is a model based on the ProtoPNet approach that uses prototypes to simulate human reasoning. Specifically, Quasi-ProtoPNet uses only a positive reasoning process, placing a zero binding across similarity scores and misclassifications. Quasi-ProtoPNet does not perform convex optimization of the last layer to maintain constant connections, in other words, the model does not freeze all other layers to optimize the last dense layer [57].

Besides the positive reasoning process, Quasi-ProtoPNet employs prototypes of all spatial dimensions, meaning rectangular and square spatial dimensions, while the ProtoPNet models generally use prototypes having only square spatial dimensions. Other models based on ProtoPNet are increasingly being used, most notable are Semi-ProtoPNet [58], Ps-ProtoPNet [59], Gen-ProtoPNet [60], and NP-ProtoPNet [61]. The Gen-ProtoPNet uses a generalized version of the Euclidean distance function, the NP-ProtoPNet considers the negative reasoning process and the positive reasoning

---

process, but it emphasizes the negative reasoning process, and the Ps-ProtoPNet equally considers both types of reasoning processes and uses fixed connections between similarity scores and logits.

Quasi-ProtoPNet has convolution layers of a base model that are followed by two additional convolution layers, here the VGG-16, VGG-19, ResNet-34, ResNet-152, DenseNet-121, and DenseNet-16 are used as baselines. The convolutional layers are denoted by L, and are followed by a generalized convolutional layer p_t of prototypical parts. The p_t layer is followed by a dense w layer, without bias. The weight matrix of the dense layer is, respectively, denoted by w_m. In this structure, the L convolutional layers are the non-interpretable part of the Quasi-ProtoPNet (Figure 1e), while the p_t forms the interpretable part of the model (Figure 1f).

Quasi-ProtoPNet employs the generalized version of the Euclidean distance function (d). Since p is any prototype with the shape $512 \times h \times w$, wherein $1 \leq h, w \leq 6$, and h and w together are not equal to 1 nor 6. The model output $\mathcal{O}(= L(x))$ of L has $(7 - h)(7 - w)$ patches of dimensions $h \times w$. Therefore, the square of the distance is $d(\mathcal{P}_{ij}, p)$ between p and (i, j) patch $\mathcal{P}_{ij}$ of $\mathcal{O}$ is given by:

$$d^2(\mathcal{P}_{ij}, p) = \sum_{l=1}^{h} \sum_{m=1}^{w} \sum_{k=1}^{512} ||\mathcal{O}_{(i+l-1)(j+m-1)k} - p_{lmk}||_2^2. \quad (2)$$

If p has prototypes of spatial dimensions 1×1 ($h = w = 1$),

$$d^2(\mathcal{P}_{ij}, p) = \sum_{k=1}^{512} ||\mathcal{O}_{ijk} - p_{11k}||_2^2, \quad (3)$$

which is the Euclidean distance square between p and a patch of $\mathcal{O}$, in which $p_{11k} \simeq p_k$. The prototypical unit p_t computes

$$p_t(\mathcal{O}) = \max_{1 \leq i \leq 7-h,\ 1 \leq j \leq 7-w} \log \left(\frac{d^2(\mathcal{P}_{ij}, p) + 1}{d^2(\mathcal{P}_{ij}, p) + \epsilon} \right). \quad (4)$$

Thus,

$$p_t(L(x)) = \max_{\mathcal{P} \in \text{patches}(L(x))} \log \left(\frac{d^2(\mathcal{P}, p) + 1}{d^2(\mathcal{P}, p) + \epsilon} \right). \quad (5)$$

The Quasi-ProtoPNet is trained using two steps, the optimization of all layers before the dense layers, and the projection of prototypes [57]. Given $X = \{x_1 \dots x_n\}$ and $Y = \{y_1 \dots y_n\}$ are, respectively, sets of images and labels, and

$$D = \{(x_i, y_i) : x_i \in X, y_i \in Y\}, \quad (6)$$

the objective function of the Quasi-ProtoPNet is:

$$\min_{P, L_{conv}} \frac{1}{n} \sum_{i=1}^{n} \text{CrosEnt}(h \circ p_t \circ L(x_i), y_i) + \lambda \text{ClstCost}, \quad (7)$$
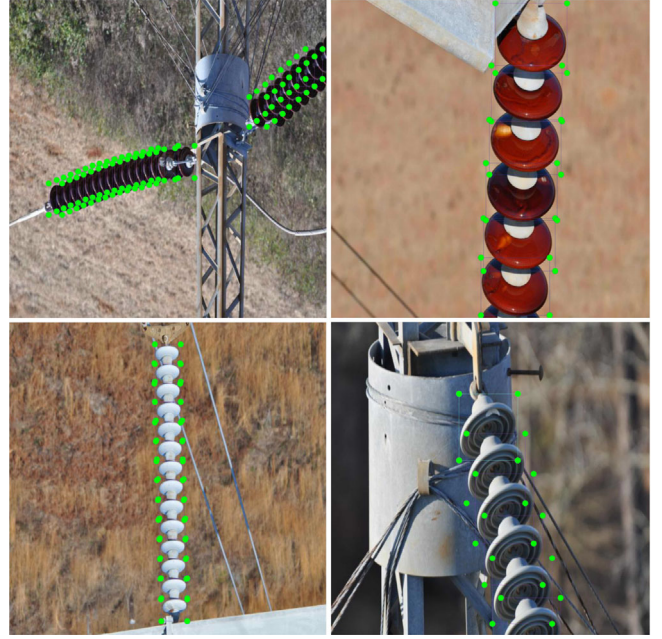

FIGURE 2 Annotated images from the used dataset [63].

where the cluster cost (ClstCost) is given by:

$$\text{ClstCost} = \frac{1}{n} \sum_{i=1}^{n} \min_{j : p_j \in P_{y_i}} \min_{\mathcal{P} \in \text{ patches}(L(x_i))} d^2(\mathcal{P}, p_j). \quad (8)$$

Considering x is an input image, the model projects prototypes over patches of x which are more similar to the prototypes [62]. Therefore, a patch of x is projected that is at a smaller distance from a prototype, given the following update:

$$p_j^c \longleftarrow \arg \min_{\{\mathcal{P} : \mathcal{P} \in \text{patches}(L(x_i))\ \forall i \text{ such that } y_i = c\}} d(\mathcal{P}, p_j^c). $$

3.3 | Dataset

The used dataset was created by Lewis and Kulkarni [63], for a competition with the goal of insulator defect detection. The dataset has high-quality labeled images of transmission line insulators, which contain four classes: insulators with flashover, broken insulators, good insulators, and insulator chains. Since the purpose of this paper is to classify the condition of insulators (faulty and good), the insulator chain class was disregarded. Some of the insulators from this database are shown in Figure 2.

The database contains high-resolution pictures of porcelain insulator chains from power lines, on which the positions and classes of insulators are noted according to bounding boxes regarding the vertical and horizontal position and their condition. The images were recorded using digital single-lens reflex cameras (DSLRs) during aerial inspections of the electrical power grid. The DSLRs settings were adjusted according to the need for brightness compensation, considering the use of the Canon PowerShot G10, Nikon D810, and Nikon D90.

The dataset has 1596 images, wherein 1195 were used during the training, and 401 for testing. The high-resolution images are rescaled to 640 pixels on input to the model to have standard images according to the training needs of the presented architecture.

The cutouts considered for the classification task were 10,886 for training and 1941 for testing, divided as follows: Broken class (train: 877, test: 191), flashover class (train: 1651, test: 288), and good class (train: 8358, test: 1462). The cutouts have varying resolutions according to the bounding boxes of the insulator. After augmented data, the dataset has thirty times the original number of images (broken: 26,310, flashover: 49,530, good: 250,740).

3.4 | Experiment setup

The purpose of the present experiment is to compare object detection and classification models to determine the best framework for identifying insulator failures in transmission grids. The measures of object detection performance here were precision, recall, F1-score, and mAP. The positive predictive value (precision) and the sensitivity (recall) are given by:

$$\text{Precision} = \frac{tp}{tp + fp}, \tag{9}$$

$$\text{Recall} = \frac{tp}{tp + fn}. \tag{10}$$

These measures are obtained from the confusion matrix considering the true positive (tp), false positive (fp), and false negative (fn). From the precision and recall, the F1-score is obtained, according to:

$$\text{F1}-\text{score} = \frac{2 \times \text{Precision} \times \text{Recall}}{\text{Precision} + \text{Recall}}. \tag{11}$$

The intersection over union (IoU) determines when detection is considered a true positive. A detection of tp is defined by $IoU > T$, in which T is a predefined threshold. Here, the valuation is made by T equal to 0.5. To evaluate the object detection, the mAP was used, given by:

$$\text{mAP} = \frac{1}{n} \sum_{k=1}^{n} AP_k, \tag{12}$$

where n is the number of classes and k is the corresponding class. The average precision (AP) calculates a precision–recall curve as the weighted average of the precision achieved for each threshold.

The method proposed here was implemented using Python language. To perform the training and comparative analysis, a cluster was used, in which the following setup requirements were allocated: A graphic processing unit (GPU) GeForce GTX 1080 Ti, and 64 GB of random access memory (RAM). This hardware setup was used since it was sufficient to compute all the experiments and thus facilitate reproducibility. To evaluate the computational effort, floating-point operations (FLOPs) are used.

For the object detection task, the nano, small, medium, large, extra-large, and ultra-large versions of the YOLOv5, of which are YOLOv5n, YOLOv5s, YOLOv5m, YOLOv5l, YOLOv5x, and YOLOv5u are evaluated. These versions were based on 640-pixel images and the difference between them is the number of layers and parameters. These variations in size are given by the depth and width multiple of the network. Especially the ultra-large version is not available in Ultralytics models, the YOLOv5u was created based on increasing both the layers and the parameters of the network, this is a customized version created here for comparison to the standard models.

All compared models presented here were trained from scratch to have an equivalent condition for comparison. Since the models were trained from scratch a maximum value of 10,000 epochs for training was defined, considering that in the initial experiments, the models converged before 1000 epochs, to improve the development of the analysis the early stopping patience was used, in which the model ends the training if there are 50 epochs without improvement.

4 | RESULTS AND DISCUSSION

Whereas the proposed model uses a personalized ultra-large version for object detection (YOLOv5u), the first analysis step is to define the appropriate structure size of the network. At this stage of the analysis, all annotated insulators are considered to be of the same class, in view that YOLOv5u is used for object detection, and Quasi-ProtoPNet is used specifically for classification. The results of object detection concerning the variation in the size of the network are presented in Table 1.

Since YOLOv5u is trained from scratch, it is needed to set a higher maximum value of epochs, 10,000 here, which is considerably more than the standard 300 epochs suggested in the model's original repository. Considering the used early stop criteria, the compared models converged at close to 1000 epochs. Here, the best results of comparative analyzes between models of the same class are underlined and the best overall results are highlighted in bold.

In this initial comparison, all the models were able to achieve F1-score results above 0.97, which shows that the approach is feasible for the application in question. As expected, the models that have more parameters need more time to be computed due to the higher computational effort required, which can also be observed by the higher value of FLOPs.

The mAP@[0.5] was greater than 0.98 in all compared models, showing that object detection is successfully performed using YOLOv5 in all its versions. Considering the F1-score result the model that presented the best result was YOLOv5u (1.50_1.67) using 465 layers and 158.5 million parameters. For this reason, this structure has been defined as the standard model for object detection, since at this stage of the analysis all the insulators are considered equal because the objective of the YOLOv5 model is to locate the components for further classification by the Quasi-ProtoPNet model.

**TABLE 1** Definition of structure for object detection.

Model	*depth_width*	Layers	Parameters (M)	FLOPs (G)	Time (s)	Precision	Recall	F1-score	mAP [0.5]	[0.5:0.95]
YOLOv5n	0.33_0.25	213	1.9	4.5	27,884.0	0.98092	0.96806	0.97445	**0.98757**	0.84610
YOLOv5s	0.33_0.50	213	7.2	16.5	28,477.8	0.97797	0.97424	0.97610	0.98720	0.88088
YOLOv5m	0.67_0.75	290	21.2	49.0	38,551.6	0.97949	0.97372	**0.97659**	0.98492	0.89924
YOLOv5l	1.00_1.00	367	46.5	109.1	60,093.9	0.97526	0.97527	0.97526	0.98483	**0.91291**
YOLOv5x	1.33_1.25	444	86.7	205.7	74,945.3	0.98120	0.96815	0.97463	0.98271	0.91187
YOLOv5u	1.33_1.50	444	124.1	293.0	133,823.4	**0.98110**	0.97269	0.97688	0.98353	0.91191
	1.50_1.50	465	127.4	307.2	139,318.1	0.97774	0.97311	0.97542	0.98333	0.91234
	1.50_1.67	465	158.5	384.6	182,122.8	0.98057	**0.97476**	**0.97765**	0.98314	0.90545
	1.67_1.67	521	179.7	431.9	190,239.1	0.97411	**0.97476**	0.97443	0.98260	0.91248
	1.67_1.75	521	196.6	469.0	272,763.3	0.97375	0.97372	0.97373	**0.98420**	**0.91679**

The difference between the YOLOv5 (1.50_1.67) which had the best F1-score result to the YOLOv5n, which uses fewer parameters, was 0.0032. YOLOv5n had the best mAP@[0.5] results, lower time to be computed, and higher efficiency considering the FLOPs, however, it had the lowest mAP@[0.5:0.95] value. This shows that depending on the research objective, smaller models can have an acceptable F1-score and even be better in some circumstances relative to mAP@[0.5].

The time required for training increases when the model uses more parameters, the difference between the model that used a *depth_width* equal to 1.67_1.75 to the YOLOv5n was approximately 10 times more time to complete the training. Although the training time was higher, all models needed less than 3 ms to process each image during the testing phase. This makes their application in embedded systems promising since in the testing phase the computational effort may be limited and a fast response is required.

The output of the YOLOv5u model provides the position of the insulator and based on an image cutout of where the insulator is, the classification of the component is performed. To perform an optimization on the structure of the Quasi-ProtoPNet, the VGG-16, VGG-19, ResNet-34, ResNet-152, DenseNet-121, and DenseNet-161 baselines are evaluated. Table 2 shows the classification results using the Quasi-ProtoPNet model considering this variation, and compares with well-established models. In this evaluation, mAP values are not presented as this metric is based on the IoU of object detection that was previously presented in Table 1 for the YOLOv5u model. Therefore, Quasi-ProtoPNet is focused specifically on the classification task.

The Quasi-ProtoPNet is superior to all compared models using all backbone variations for the classification task presented here. Using the DenseNet-161 as the backbone, the Quasi-ProtoPNet had an F1-score of 0.95165 being promising for the classification of insulators. These results confirm that using Quasi-ProtoPNet from the object detection performed by YOLOv5u via a hybrid method defined as YOLOu-Quasi-
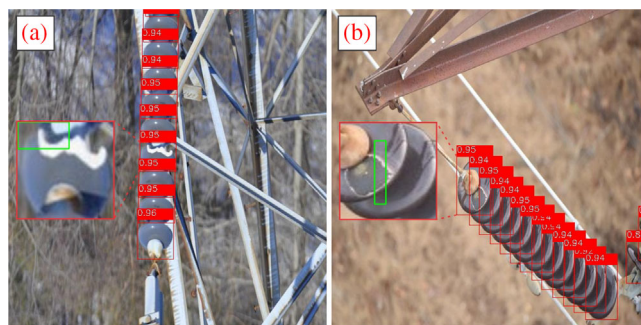
FIGURE 3 Testing images results: (a) Broken insulator; (b) Flashover insulator.

ProtoPNet is a good strategy for the evaluation in question. Figure 3 shows examples of results with inference images (not used in training) using the proposed method.

In Figure 3a, a broken insulator is presented, and in Figure 3b an insulator with a flashover over its surface is presented. These failures are the most common to be identified in a power grid inspection and are the focus of the application of the proposed method.

4.1 | Comparison to related studies

Serikbay et al. [64] using a starting CNN had an accuracy of 0.8907 in the testing phase. In this application only 1.38 MB of memory was required, making this a promising solution to be applied in an embedded system. Alahyari et al. [65] used a two-stage model for both the segmentation and the detection tasks of faulty insulators. The segmentation model achieved a total of 78% accuracy, while the classifier obtained 92%. When the data is unbalanced the accuracy may not be enough to determine whether the model is having an acceptable classification result.

Zhang et al. [66] used a Fast R-CNN network to identify insulator strings. Regarding the detection of the insulator strings, the

**TABLE 2**　Comparison of the Quasi-ProtoPNet with different baselines to well-established models.

Base	Metric	Quasi-ProtoPNet [57]	Semi-ProtoPNet [58]	Ps-ProtoPNet [59]	Gen-ProtoPNet [60]	NP-ProtoPNet [61]	ProtoPNet [62]
VGG-16	Precision	0.89552	0.67187	0.68749	0.56870	0.712499	0.75590
	Recall	0.85714	0.23369	0.34591	0.30483	0.31232	0.28318
	F1-score	0.87591	0.34677	0.46025	0.39691	0.43428	0.41201
VGG-19	Precision	0.95628	0.51464	0.71249	0.57419	0.57142	0.57516
	Recall	0.86206	0.38317	0.31232	0.26567	0.31901	0.25882
	F1-score	0.90673	0.43928	0.43428	0.36326	0.40944	0.35699
ResNet-34	Precision	0.95767	0.89893	0.88324	0.58139	0.85572	0.58778
	Recall	0.88292	0.75446	0.77678	0.26041	0.77477	0.18075
	F1-score	0.91878	0.82038	0.82660	0.35971	0.81323	0.27648
ResNet-152	Precision	0.94764	0.77725	0.74774	0.744075	0.76146	0.74999
	Recall	0.89603	0.72246	0.75113	0.69162	0.73127	0.73008
	F1-score	0.92111	0.74885	0.74943	0.71689	0.74606	0.73991
DenseNet-121	Precision	0.95897	0.89839	0.87570	0.77102	0.78095	0.71098
	Recall	0.92118	0.74666	0.68281	0.72368	0.73214	0.57209
	F1-score	0.93968	0.81553	0.76732	0.74660	0.75576	0.63402
DenseNet-161	Precision	**0.96891**	0.74404	0.68965	0.65868	0.68452	0.56544
	Recall	**0.93499**	0.43554	0.42105	0.37414	0.40069	0.41221
	F1-score	**0.95165**	0.54945	0.52287	0.47722	0.50549	0.47682

algorithm achieved an AP of 91.75% and a recall of 98%, and accuracy of 98% for the classification task. Sadykova et al. [49] used YOLOv2 to identify the string of insulators, and then a classification model to analyze the insulator surface conditions. The YOLOv2 model achieved an mAP above 98% for detecting insulator strings and an F1-score of 0.95165. Showing that even the most previous versions can be successfully used for the presented task. Comparatively, the proposed method presented here achieved similar values of F1-score and mAP, however using high-resolution images.

In reference [53], an mAP of 0.99262 was achieved considering only the task of insulator identification, based on the ResNet-18 classifier they have an F1-score result of 0.96216. Based on ResNet-34 in reference [15] an accuracy of 0.9979 and an F1-score of 0.9964 was achieved for a similar task. As can be verified, authors who have used CNN-based models have had promising results in fault identification, with the choice of model and its fine-tuning depending on the used dataset.

4.2 | Limitations

Quasi-ProtoPNet gives better performance than the series of ProtoPNet models when classification is to be made over only a few classes. If the number of classes is large then the performance of the other ProtoPNet models may be better than the Quasi-ProtoPNet. However, there are many cases similar to the case of insulators discussed here when it is needed to classify
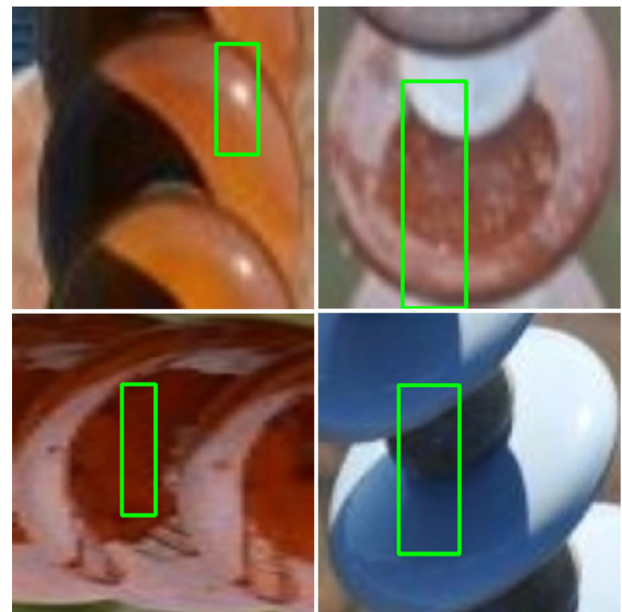
FIGURE 4　False positive classification samples.

images over only a few classes. Therefore, this model can be really useful for such situations.

In the interpretable results, there were cases where Quasi-ProtoPNet highlighted the variation in brightness intensity for good insulators, these false positives are presented in Figure 4.

Considering that these images were classified as insulators in good condition the interpretability should not be considered for non-faulty insulators.

The final result has the accumulated error of the identification based on YOLOv5u, therefore for the method to have acceptable results, it needs to have the identification of the components properly, since the classifier will not be able to classify failures if the component is not identified.

5 | FINAL CONSIDERATIONS

The proposal of using Quasi-ProtoPNet as a classifier instead of using only YOLO had rewarding results, comparatively, Quasi-ProtoPNet was superior in using different baselines to all other compared models based on ProtoPNet, additionally, YOLOv5u showed promise for object detection, hence the proposed hybrid optimized YOLOu-Quasi-ProtoPNet excelled in all comparisons for solving the problem presented here.

The use of YOLOv5 specifically for detecting insulators had superior results to its use for identifying different conditions, this means that the task of detecting these components may be simpler than their classification. This result is reflected in electrical grid inspections, where the insulator chain is easily identified, even by people without specific training, but the identification of a failure requires advanced training and knowledge of the grid conditions. Numerically, all variations of the YOLOv5 model had an F1-score higher than 0.97 and an mAP@[0.5] higher than 0.98 for insulator detection, while the best results of these models were an F1-score of 0.93986 and an mAP@[0.5:0.95] of 0.87312 (*depth_width* of 1.33_1.50) when it was necessary to identify the insulator condition, making it clear that the use of a hybrid method for classification is a promising strategy.

Considering that several state-of-the-art models have been evaluated and combined, in future work, it would be promising to employ these models in embedded systems, where a specific device could indicate fault conditions to a maintenance team in the field. This would support the correction of failures that occur suddenly, thereby indicating adverse conditions for a team to identify the failure and correct it more dynamically when a shutdown occurs. The YOLO model is being explored and improved over time, new versions have been made available such as YOLOv6, YOLOv7, and more recently YOLOv8. Based on the promising results of using models larger than the extra-large version of YOLO, it becomes interesting to further increase the number of parameters of the model to obtain an ultra-large version of the latest YOLO structures.

CONFLICT OF INTEREST STATEMENT
The authors declare no conflict of interest.

DATA AVAILABILITY STATEMENT
The data are available upon request to the authors.

ORCID
Stefano Frizzo Stefenon https://orcid.org/0000-0002-3723-616X

REFERENCES
1. Dong, B., Hu, Y., Yin, F., Jiang, X.: Simulation calculation of 3D electric field and natural flashover analysis of ice-covered silicone rubber insulator. IET Gener. Transm. Distrib. 17(5), 1166–1178 (2023)
2. Mohammadnabi, S., Rahmani, K.: Influence of humidity and contamination on the leakage current of 230-kV composite insulator. Electr. Power Syst. Res. 194, 107083 (2021)
3. Salem, A.A., Abd-Rahman, R., Ishak, M.T.B., Lau, K.Y., Abdul-Malek, Z., Al-ameri, S., et al.: Influence of contamination distribution in characterizing the flashover phenomenon on outdoor insulator. Ain Shams Eng. J. 102249 (2023)
4. Salem, A.A., Lau, K.Y., Abdul-Malek, Z., Al-Gailani, S.A., Tan, C.W.: Flashover voltage of porcelain insulator under various pollution distributions: Experiment and modeling. Electr. Power Syst. Res. 208, 107867 (2022)
5. Stefenon, S.F., Corso, M.P., Nied, A., Perez, F.L., Yow, K.C., Gonzalez, G.V., et al.: Classification of insulators using neural network based on computer vision. IET Gener. Transm. Distrib. 16(6), 1096–1107 (2022)
6. Stefenon, S.F., Bruns, R., Sartori, A., Meyer, L.H., Ovejero, R.G., Leithardt, V.R.Q.: Analysis of the ultrasonic signal in polymeric contaminated insulators through ensemble learning methods. IEEE Access 10, 33980–33991 (2022)
7. Medeiros, A., Sartori, A., Stefenon, S.F., Meyer, L.H., Nied, A.: Comparison of artificial intelligence techniques to failure prediction in contaminated insulators based on leakage current. J. Intell. Fuzzy Syst. 42(4), 3285–3298 (2022)
8. Salem, A.A., Abd-Rahman, R., Rahiman, W., Al-Gailani, S.A., Al-Ameri, S.M., Ishak, M.T., et al.: Pollution flashover under different contamination profiles on high voltage insulator: Numerical and experiment investigation. IEEE Access 9, 37800–37812 (2021)
9. Sopelsa Neto, N.F., Stefenon, S.F., Meyer, L.H., Bruns, R., Nied, A., Seman, L.O., et al.: A study of multilayer perceptron networks applied to classification of ceramic insulators using ultrasound. Appl. Sci. 11(4), 1592 (2021)
10. Zhang, D., Zhang, Z., Jiang, X., Zhang, W., Zhao, J., Bi, M.: Influence of fan-shaped non-uniform pollution on the electrical property of typical type HVDC insulator and insulation selection. IET Gener. Transm. Distrib. 10(14), 3555–3562 (2016)
11. Salem, A.A., Lau, K.Y., Abdul-Malek, Z., Zhou, W., Al-Ameri, S., Al-Gailani, S.A., et al.: Investigation of high voltage polymeric insulators performance under wet pollution. Polymers 14(6), 1236 (2022)
12. Deb, S., Ray Choudhury, N., Ghosh, R., Chatterjee, B., Dalai, S.: Short time modified hilbert transform-aided sparse representation for sensing of overhead line insulator contamination. IEEE Sens. J. 18(19), 8125–8132 (2018)

13. Branco, N.W., Cavalca, M.S.M., Stefenon, S.F., Leithardt, V.R.Q.: Wavelet LSTM for fault forecasting in electrical power grids. Sensors 22(21), 8323 (2022)

14. Wang, Y., Huang, L., Shahidehpour, M., Lai, L.L., Zhou, Y.: Impact of cascading and common-cause outages on resilience-constrained optimal economic operation of power systems. IEEE Trans. Smart Grid 11(1), 590–601 (2020)

15. Singh, G., Stefenon, S.F., Yow, K.C.: Interpretable visual transmission lines inspections using pseudo-prototypical part network. Mach. Vis. Appl. 34, 41 (2023)

16. Corso, M.P., Perez, F.L., Stefenon, S.F., Yow, K.C., García-Ovejero, R., Leithardt, V.R.Q.: Classification of contaminated insulators using k-nearest neighbors based on computer vision. Computers 10(9), 112 (2021)

17. Park, K.C., Motai, Y., Yoon, J.R.: Acoustic fault detection technique for high-power insulators. IEEE Trans. Ind. Electron. 64(12), 9699–9708 (2017)

18. Kim, Y., Shong, K.: The characteristics of UV strength according to corona discharge from polymer insulators using a UV sensor and optic lens. IEEE Trans. Power Delivery 26(3), 1579–1584 (2011)

19. Jin, L., Tian, Z., Ai, J., Zhang, Y., Gao, K.: Condition evaluation of the contaminated insulators by visible light images assisted with infrared information. IEEE Trans. Instrum. Meas. 67(6), 1349–1358 (2018)

20. Dong, M., Wang, B., Ren, M., Zhang, C., Zhao, W., Albarracín, R.: Joint visualization diagnosis of outdoor insulation status with optical and acoustical detections. IEEE Trans. Power Delivery 34(4), 1221–1229 (2019)

21. Stefenon, S.F., Freire, R.Z., Meyer, L.H., Corso, M.P., Sartori, A., Nied, A., et al.: Fault detection in insulators based on ultrasonic signal processing using a hybrid deep learning technique. IET Sci. Meas. Technol. 14(10), 953–961 (2021)

22. Xu, Y., Yan, X., Sun, B., Zhai, J., Liu, Z.: Multireceptive field denoising residual convolutional networks for fault diagnosis. IEEE Trans. Ind. Electron. 69(11), 11686–11696 (2022)

23. Tao, X., Zhang, D., Wang, Z., Liu, X., Zhang, H., Xu, D.: Detection of power line insulator defects using aerial images analyzed with convolutional neural networks. IEEE Trans. Syst. Man Cybernet. 50(4), 1486–1498 (2020)

24. Hao, Y., Liang, W., Yang, L., He, J., Wu, J.: Methods of image recognition of overhead power line insulators and ice types based on deep weakly-supervised and transfer learning. IET Gener. Transm. Distrib. 16(11), 2140–2153 (2022)

25. Qiu, Z., Zhu, X., Liao, C., Shi, D., Kuang, Y., Li, Y., et al.: Detection of bird species related to transmission line faults based on lightweight convolutional neural network. IET Gener. Transm. Distrib. 16(5), 869–881 (2022)

26. Stefenon, S.F., Ribeiro, M.H.D.M., Nied, A., Mariani, V.C., Coelho, L.D.S., Leithardt, V.R.Q., et al.: Hybrid wavelet stacking ensemble model for insulators contamination forecasting. IEEE Access 9, 66387–66397 (2021)

27. Stefenon, S.F., Branco, N.W., Nied, A., Bertol, D.W., Finardi, E.C., Sartori, A., et al.: Analysis of training techniques of ann for classification of insulators in electrical power systems. IET Gener. Transm. Distrib. 14(8), 1591–1597 (2020)

28. Chen, K.L., Guo, Y., Ma, X.: Contactless voltage sensor for overhead transmission lines. IET Gener. Transm. Distrib. 12(4), 957–966 (2018)

29. Xiong, S., Liu, Y., Yan, Y., Pei, L., Xu, P., Fu, X., et al.: Object recognition for power equipment via human-level concept learning. IET Gener. Transm. Distrib. 15(10), 1578–1587 (2021)

30. He, T., Zeng, Y., Hu, Z.: Research of multi-rotor UAVs detailed autonomous inspection technology of transmission lines based on route planning. IEEE Access 7, 114955–114965 (2019)

31. Waleed, D., Mukhopadhyay, S., Tariq, U., El-Hag, A.H.: Drone-based ceramic insulators condition monitoring. IEEE Trans. Instrum. Meas. 70, 1–12 (2021)

32. Salem, A.A., Abd-Rahman, R., Al Gailani, S.A., Salam, Z., Kamarudin, M.S., Zainuddin, H., et al.: Risk assessment of polluted glass insulator using leakage current index under different operating conditions. IEEE Access 8, 175827–175839 (2020)

33. Salem, A.A., Lau, K.Y., Abdul-Malek, Z., Mohammed, N., Al-Shaalan, A.M., Al-Shamma'a, A.A., et al.: Polymeric insulator conditions estimation by using leakage current characteristics based on simulation and experimental investigation. Polymers 14(4), 737 (2022)

34. Salem, A.A., Lau, K.Y., Rahiman, W., Al-Gailani, S.A., Abdul-Malek, Z., Abd-Rahman, R., et al.: Pollution flashover characteristics of coated insulators under different profiles of coating damage. Coatings 11(10), 1194 (2021)

35. Salem, A.A., Abd-Rahman, R., Rahiman, W., Al-Gailani, S.A., Al-Ameri, S.M., Ishak, M.T., et al.: Pollution flashover under different contamination profiles on high voltage insulator: Numerical and experiment investigation. IEEE Access 9, 37800–37812 (2021)

36. Stefenon, S.F., Seman, L.O., Pavan, B.A., Ovejero, R.G., Leithardt, V.R.Q.: Optimal design of electrical power distribution grid spacers using finite element method. IET Gener. Transm. Distrib. 16, 1865–1876 (2022)

37. Stefenon, S.F., Neto, C.S.F., Coelho, T.S., Nied, A., Yamaguchi, C.K., Yow, K.C.: Particle swarm optimization for design of insulators of distribution power system based on finite element method. Electr. Eng. 104, 615–622 (2022)

38. Stefenon, S.F., Americo, J.P., Meyer, L.H., Grebogi, R.B., Nied, A.: Analysis of the electric field in porcelain pin-type insulators via finite elements software. IEEE Lat. Am. Trans. 16(10), 2505–2512 (2018)

39. Dong, G., Li, Q., Liu, T., Gao, H., Zhang, M.: Finite-element analysis for surface discharge on polyimide insulation in air at atmospheric pressure under pulsed electrical stress. High Voltage 5(2), 166–175 (2020)

40. Tang, Z., Jia, C., Wang, H., Rong, S., Zhao, W.: Intelligent height measurement technology for ground encroachments in large-scale power transmission corridor based on advanced binocular stereovision algorithms. IET Gener. Transm. Distrib. 17(2), 448–460 (2023)

41. Yang, L., Fan, J., Liu, Y., Li, E., Peng, J., Liang, Z.: A review on state-of-the-art power line inspection techniques. IEEE Trans. Instrum. Meas. 69(12), 9350–9365 (2020)

42. Foudeh, H.A., Luk, P.C.K., Whidborne, J.F.: An advanced unmanned aerial vehicle (UAV) approach via learning-based control for overhead power line monitoring: A comprehensive review. IEEE Access 9, 130410–130433 (2021)

43. Jin, H., Lv, Z., Yuan, Z., Wei, Z., Wang, C., Wang, C., et al.: Micro-cracks identification and characterization on the sheds of composite insulators by fractal dimension. IEEE Trans. Smart Grid 12(2), 1821–1824 (2021)

44. Stefenon, S.F., Yow, K.C., Nied, A., Meyer, L.H.: Classification of distribution power grid structures using inception v3 deep neural network. Electr. Eng. 104, 4557–4569 (2022)

45. Mussina, D., Irmanova, A., Jamwal, P.K., Bagheri, M.: Multi-modal data fusion using deep neural network for condition monitoring of high voltage insulator. IEEE Access 8, 184486–184496 (2020)

46. Zhao, Z., Zhen, Z., Zhang, L., Qi, Y., Kong, Y., Zhang, K.: Insulator detection method in inspection image based on improved faster R-CNN. Energies 12(7), 1204 (2019)

47. Lei, X., Sui, Z.: Intelligent fault detection of high voltage line based on the faster R-CNN. Measurement 138, 379–385 (2019)

48. Guo, Y., Pang, Z., Du, J., Jiang, F., Hu, Q.: An improved AlexNet for power edge transmission line anomaly detection. IEEE Access 8, 97830–97838 (2020)

49. Sadykova, D., Pernebayeva, D., Bagheri, M., James, A.: IN-YOLO: Real-time detection of outdoor high voltage insulators using UAV imaging. IEEE Trans. Power Delivery 35(3), 1599–1601 (2020)

50. Rymarczyk, D., Struski, Ł., Górszczak, M., Lewandowska, K., Tabor, J., Zieliński, B.: Interpretable image classification with differentiable prototypes assignment. In: Computer Vision - ECCV 2022, pp. 351–368. Springer Nature, Cham, Switzerland (2022)

51. Yan, K., Li, Q., Li, H., Wang, H., Fang, Y., Xing, L., et al.: Deep learning-based substation remote construction management and AI automatic violation detection system. IET Gener. Transm. Distrib. 16(9), 1714–1726 (2022)

52. Hsu, W.Y., Lin, W.Y.: Ratio-and-scale-aware YOLO for pedestrian detection. IEEE Trans. Image Process. 30, 934–947 (2021)

53. Souza, B.J., Stefenon, S.F., Singh, G., Freire, R.Z.: Hybrid-YOLO for classification of insulators defects in transmission lines based on UAV. Int. J. Electr. Power Energy Syst. 148, 108982 (2023)

54. Tan, M., Pang, R., Le, Q.V.: Efficientdet: Scalable and efficient object detection. In: Proceedings of the IEEE/CVF conference on computer vision and pattern recognition, pp. 10781–10790 (2020)

55. Lin, T.Y., Maire, M., Belongie, S., Hays, J., Perona, P., Ramanan, D., et al.: Microsoft COCO: Common objects in context. In: European conference on computer vision. Computer Vision, pp. 740–755. Springer, Cham, Switzerland (2014)

56. Du, W., Shen, H., Fu, J.: Automatic defect segmentation in x-ray images based on deep learning. IEEE Trans. Ind. Electron. 68(12), 12912–12920 (2021)

57. Singh, G.: Think positive: An interpretable neural network for image recognition. Neural Networks 151, 178–189 (2022)

58. Stefenon, S.F., Singh, G., Yow, K.C., Cimatti, A.: Semi-ProtoPNet deep neural network for the classification of defective power grid distribution structures. Sensors 22(13), 4859 (2022)

59. Singh, G., Yow, K.C.: Object or background: An interpretable deep learning model for COVID-19 detection from CT-scan images. Diagnostics 11(9), 1732 (2021)

60. Singh, G., Yow, K.C.: An interpretable deep learning model for COVID-19 detection with chest x-ray images. IEEE Access 9, 85198–85208 (2021)

61. Singh, G., Yow, K.C.: These do not look like those: An interpretable deep learning model for image recognition. IEEE Access 9, 41482–41493 (2021)

62. Chen, C., Li, O., Tao, C., Barnett, A.J., Su, J., Rudin, C.: This looks like that: Deep learning for interpretable image recognition. arXiv 5, 1–12 (2019)

63. Lewis, D., Kulkarni, P.: Insulator defect detection. IEEE Dataport (2021). https://www.doi.org/10.21227/vkdw-x769

64. Serikbay, A., Bagheri, M., Zollanvari, A., Phung, B.T.: Accurate surface condition classification of high voltage insulators based on deep convolutional neural networks. IEEE Trans. Dielectr. Electr. Insul. 28(6), 2126–2133 (2021)

65. Alahyari, A., Hinneck, A., Tariverdizadeh, R., Pozo, D.: Segmentation and defect classification of the power line insulators: A deep learning-based approach. In: 2020 International Conference on Smart Grids and Energy Systems (SGES), pp. 476–481. IEEE, New York (2020)

66. Zhang, Z., Huang, S., Li, Y., Li, H., Hao, H.: Image detection of insulator defects based on morphological processing and deep learning. Energies 15(7), 2465 (2022)